Intraband Dynamics and Exciton Trapping in the LH2 Complex of Rhodopseudomonas acidophila

*Erling Thyrhaug[1], Marco Schröter[2, 3], Eglė Bukartė[2], Oliver Kühn[3], Richard Cogdell[4], Jürgen Hauer[1], Donatas Zigmantas[2]**

[1] Dynamical Spectroscopy, Department of Chemistry, Technical University of Munich, Lichtenbergstrasse 4, 85748 Garching b. Munich, Germany

[2] Chemical Physics, Department of Chemistry, Lund University, P.O. Box 124, SE-22100 Lund, Sweden

[3] Institute of Physics, University of Rostock, Albert Einstein Straße 23-24, 18059 Rostock, Germany.

[4] Institute of Molecular, Cell and Systems Biology, University of Glasgow, Room 402, Davidson Building, Glasgow G12 8QQ, Scotland

*** Author to whom correspondence should be addressed**: donatas.zigmantas@chemphys.lu.se

ABSTRACT

Over the last several decades, the light-harvesting protein complexes of purple bacteria have been among the most popular model systems for energy transport in excitonic systems in the weak and intermediate intermolecular coupling regime. In spite of this extensive body of scientific work, significant questions regarding the excitonic states and the photoinduced dynamics remain. Here, we address the low-temperature electronic structure and excitation dynamics in the light harvesting complex 2 (LH2) of *Rhodopseudomonas (Rh.) acidophila* by 2D electronic spectroscopy. We find that, although energy relaxation is very rapid, exciton mobility is limited over a significant range of excitation energies. This points to the presence of a sub-200 fs, spatially local energy relaxation mechanism, and suggests that local trapping might contribute substantially more in cryogenic experiments than under *physiological* conditions where the thermal energy is comparable to- or larger than- the static disorder.

INTRODUCTION

In the photosynthetic apparatus of algae, plants and many bacterial species, captured solar energy is utilized to fuel the chemical transformation of carbon dioxide and water into carbohydrates and oxygen. This process requires, in terms of energy, approximately 3-4 visible or near infrared photons per molecule of oxygen produced. This large energy demand presents a strong potential bottleneck in the energy-conversion of biological reaction centers. In fact, under natural light conditions, the absorption rate of any single photosynthetic reaction center would be much too slow to serve as a viable energy source for the organism[1, 2]. Photosynthetic organisms circumvented this bottleneck by addition of large antennae, comprising of tens to thousands of chlorophylls, to the functional units of the photosynthetic apparatus[3]. These light-harvesting antennae are tasked with serving excitation energy to the reaction centers, which is accomplished by a combination of very large absorption cross-section and efficient energy transport. In the majority of phototropic organisms,

the antennae chromophores are held in specific and well-defined spatial arrangements by a protein matrix to form pigment-protein complexes - the light harvesting antenna complexes (LHCs)[4].

LHCs appear in a great variety both in terms of pigment content and structure[1], however most of them perform their designated tasks exceptionally well. As such, they have been intensely studied not only in the context of biological functionality[5], but have also acted as model systems in a wide range of fundamental studies concerning excitation delocalization[6], interplay between electronic and vibrational degrees of freedom[7, 8], and energy transport in molecular aggregates[9, 10]

The LHCs of purple bacteria have been especially popular and well-studied systems during the last several decades[11, 12]. The interest in these LHCs in particular, whether in the context of biological photophysics or fundamental studies of soft-matter exciton dynamics, has been at least partly motivated by the following factors[1]: *i)* they are relatively small, allowing *e.g.* detailed theoretical work, *ii)* crystal structures are known for a number of species, *iii)* a very high degree of symmetry aids in spectroscopic classification, *iv)* although they are membrane proteins, extraction into surfactant-stabilized solution is possible, *v)* unusually high photostability for biological complexes, facilitating laser spectroscopy investigations. While focusing on such practical issues might suggest that these LHCs are scientifically less important, this has certainly been proven not to be the case. On the contrary, the detailed studies made possible by these practical factors have revealed rich excited-state structures and dynamics, with many results aiding understanding of dynamics in intermediate-coupling systems – where electronic coupling is both non-negligible and comparable to system-bath coupling - in addition to obtaining the functional information.

While purple bacteria have been of interest for much longer, correlations between detailed spectroscopic and theoretical work on the protein constituents of these photosystems in particular gained traction in the mid 90ies[13] after Cogdell and coworkers determined the crystal structure of the peripheral antenna of the bacterium *Rh. acidophila*. This LHC, referred to as light-harvesting complex 2 (LH2), is primarily tasked with increasing the absorption cross-section of the core antenna-reaction center complex (LH1-RC) of the bacterium. This is achieved through efficient light absorption followed by remarkably efficient energy transport towards the LH1-RC. The LH2 pigment-protein complex consists of repeating polypeptide heterodimers, referred to as the αβ heterodimer unit. Each αβ unit non-covalently binds three bacteriochlorophyll a (BChl a) pigments – a strongly coupled BChl a dimer and one BChl a oriented approximately perpendicular to the dimer, and hence only weakly electronically coupled. Additionally, each αβ unit binds a carotenoid – in the case of *Rh. acidophila* rhodopin glucoside.

In the functional LH2 complex of *Rh. acidophila*, 9 of these αβ heterodimers assemble into a roughly circular arrangement with formally C_9 point group symmetry. As a result of this assembly, the BChl a pigments contained in the αβ units organize into two concentric rings – one consisting of nine strongly coupled BChl a dimers (thus 18 pigments in total), and one of nine weakly coupled BChl a monomers. These pigment structures are referred to as the B850 and B800 rings, respectively.

While the photoinduced dynamics in these rings have been extensively studied[14-16], several open questions remain on energy transfer dynamics and structure-function relation, especially on the role of disorder. In particular, the high density of states resulting from the relatively large number of coupled pigments offer practical problems in spectrally resolving the relaxation dynamics. At the same time, the interplay between high formal symmetry – suggesting essentially completely

delocalized and degenerate states – and localization, due to substantial dynamic and static disorder, complicates interpretation of experimental data.

Here we apply polarized two-dimensional electronic spectroscopy (2DES), supported by ultrafast degenerate transient absorption (TA) spectroscopy and steady-state spectroscopy, to follow the photoinduced dynamics in LH2 on timescales from tens of femtoseconds to tens of picoseconds at 77 K. The simultaneous spectral- and high temporal- resolution of these techniques provides a robust picture of the electronic structure and relaxation dynamics in this pigment-protein complex, with particular focus on *intra*band dynamics. Based on the agreement between global analysis of excitation-frequency dependent dynamics, extracted from electronic 2D spectra, and transient anisotropy measurements we arrive at a consistent overall picture for ultrafast dynamics in both the B800 and B850 rings.

RESULTS AND DISCUSSION

Optical Spectroscopy of the LH2 Complex from Purple Bacteria

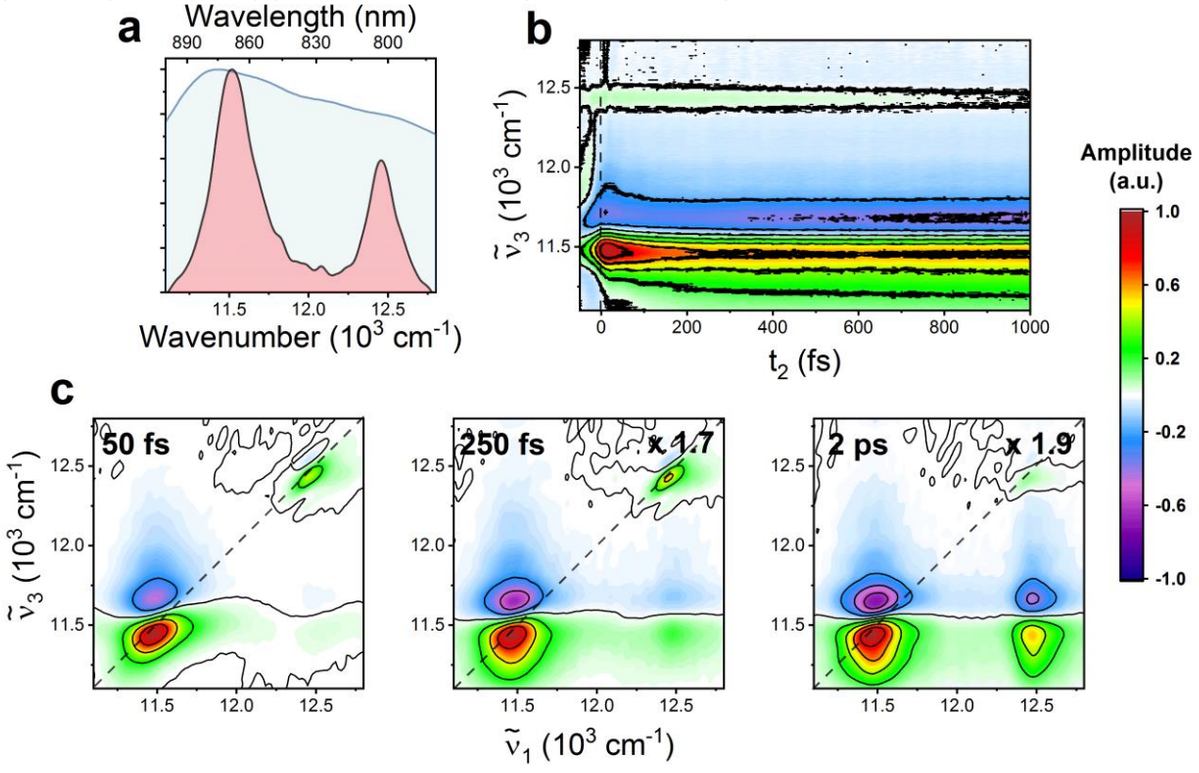

Figure 1: a) Absorption spectrum of LH2 from *Rh. acidophila* at 77K in a 1:2 buffer:glycerol mixture (red). The laser spectrum used in the ultrafast experiments is shown in blue. **b)** Broadband degenerate TA showing the pump-induced dynamics over the first picosecond. **c)** Normalized total absorptive (real) 2DES spectra at several population times demonstrate both intraband relaxation and B800→B850 energy transfer. Ground-state bleach and stimulated emission are shown with positive amplitude, while excited-state absorption is shown with negative amplitude. Both 2DES and TA experiments recorded at magic-angle polarization (MA) conditions.

The LH2 complex has a characteristic near-IR absorption spectrum – shown in Figure 1a - consisting predominantly of two intense and well-defined, but fairly broad absorption features around 800 nm and 850 nm. As implied by the naming convention, these features originate from the weakly coupled 9-member B800 ring and the strongly coupled 18-member ring B850. The sparse spectral structure

is deceptively simple, as the underlying electronic structure is not straightforward due to a combination of high formal symmetry and significant (static- and dynamic-) disorder. It is clear, however, that due to the broadness of the spectra and the relatively large number of equivalent pigments contributing, it is necessary to consider both electronic structure and relaxation in terms of bands of states rather than the discrete state-to-state transfer more common in other pigment-protein complexes.

Degenerate TA, shown in Figure 1b, qualitatively supports this picture: during excitation-triggered time evolution, we observe a rapid loss of amplitude in the B850 spectral region on a timescale of 40 fs, followed by a continuous shift of the signal towards lower energies over the next few hundred fs. This stands in contrast to the more common well-defined level-to-level transfer observed in discrete-state systems studied at cryogenic temperature. Continuous band-shift-like dynamics in the B800 region are much more subtle, as the dominating contribution is signal loss due to B800->B850 energy transfer on a timescale of approximately 1 ps (see supplementary Figure S1).

While rich in content, the TA data suffers from spectral congestion and therefore detailed information is difficult to extract unambiguously. As the relaxation dynamics are very fast, particularly in the B850 region, the short laser pulses required for sufficient temporal resolution precludes high spectral resolution. This problem is to a large degree alleviated in the 2DES spectra shown in Figure 1c, where both the ultrafast intraband dynamics and the picosecond interband transfer appears much more clearly. TA and 2DES experiments in general contain the exact same nonlinear response signals, however due to the much lower degree of spectral congestion, in the following sections we predominantly focus on analyzing 2DES data.

Electronic Structure Considerations

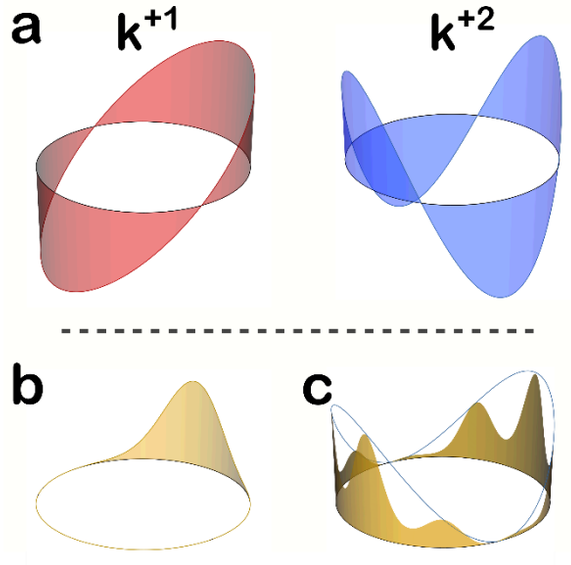

Figure 2: a) Schematic illustrations of (the real part of-) delocalized Bloch-waves on a smooth ring (u(**r**) = 1**)**. Shown are one of the degenerate dipolar states (k^{+1}) and one quadrupolar state (k^{+2}). **b)** Schematic illustration of a partly localized exciton on the same ring. **c)** Probability density of a coherent superposition of nine equivalent, small excitons distributed on a ring (yellow shaded area). Coefficients are weighted by the angle between exciton transition dipole moment and the polarization vector of an exciting field. The probability density of the $k^{+/-1}$ Bloch waves are shown as a blue line.

Some terminology used in discussion of the optical response may lead to confusion, especially among non-specialists: largely delineated by the field of expertise, qualitatively different pictures of the excited states in molecular aggregates are being used – as they appear appropriate under different experimental circumstances. In order to decrease ambiguity in the interpretation of our experimental results, we here make some brief remarks on some issues regarding the electronic structure and dynamics in purple bacteria LHCs.

The B850 excited states are frequently discussed in terms of Bloch waves[17-19], where the wavefunction takes the form $\psi(\boldsymbol{r}) \propto e^{i\boldsymbol{k}\boldsymbol{r}}u(\boldsymbol{r})$, where $u(\boldsymbol{r})$ is a periodic function. The nine-fold symmetry then requires two manifolds of - in total - eight doubly degenerate states (classified by their momentum $k^{(+/-)n}$) flanked by the totally symmetric k^0 and k^9 states[17]. As illustrated in the simplified depiction in Figure 2a, these states are delocalized over all pigments in the ring. Within the dipole approximation, only the $k^{+/-1}$ states carry significant oscillator strength due to optical selection rules. This picture, being in principle identical to the exact electronic structure in the absence of disorder, has been much used in explaining *e.g.* high-resolution- and single-molecule excitation-spectra[20]. Further support for this model has come from non-linear absorption experiments, which similarly suggested essentially complete delocalization of the optically active states in B850[21].

While the Bloch models delocalization over the entire B850-ring explain the absorption spectrum, the description of transient spectral dynamics is usually in terms of smaller excitons (or *e.g.* polarons[22, 23]), localized in a limited spatial region of the ring as schematically illustrated in Figure 2b. Here, it is presumed that any dynamics after approximately 100 fs after pulsed excitation is best described by a partially localized exciton wavefunction[24], involving only a limited number of pigments. Accordingly, the "small exciton" interpretation of B850 dynamics is based on the fact that disorder in pigment energies and coupling to the bath localize the eigenstates. While the exact spatial extent of the excitons is still not entirely settled, the estimated disorder is comparable to the electronic coupling, and excitons delocalized over approximately four[25, 26] or somewhat more[27] pigments are commonly assumed. The small-exciton picture has been confirmed (although not necessarily accurately in terms of exact delocalization length) by e.g. exciton-exciton annihilation experiments[28].

Even though the Bloch model and the moderate-size excitonic model for electronic states in LH2 are seemingly widely different, they are indeed connected. The Bloch model and the excitonic model apply to times short and long with respect to electronic dephasing [6, 29]. In particular, excitation with laser pulses short enough to follow the ultrafast dynamics in these systems inevitably creates a coherent superposition of all optically active states – an excitonic wavepacket. This is simply a consequence of the broad spectral bandwidth of these pulses, making selection of a single "small-exciton" transition impossible. As schematically illustrated in Figure 2c, the excitonic wavepacket will be delocalized over a large extent of the B850 ring, resembling a Bloch wave. The dephasing of this initial wavepacket into more localized excitons is associated with distinct observables: in particular, one expects a substantial loss of the signal strength in conjunction with depolarization of the signal on timescales commensurate with the sub-100 fs electronic dephasing times expected given the absorption linewidth. This has indeed been observed in ultrafast TA experiments[24, 30].

Besides this dynamic localization, other processes such as exciton self-trapping and polaron formation[22, 31-33] have been suggested to influence excited state dynamics in LH2. In essence, both

exciton self-trapping and polaron formation lead to an electronic state structure that can change significantly in character as a function of time. We discuss these phenomena as possible causes for the observed spectroscopic features in the following sections.

Dynamics in the Weakly-Coupled B800 Ring

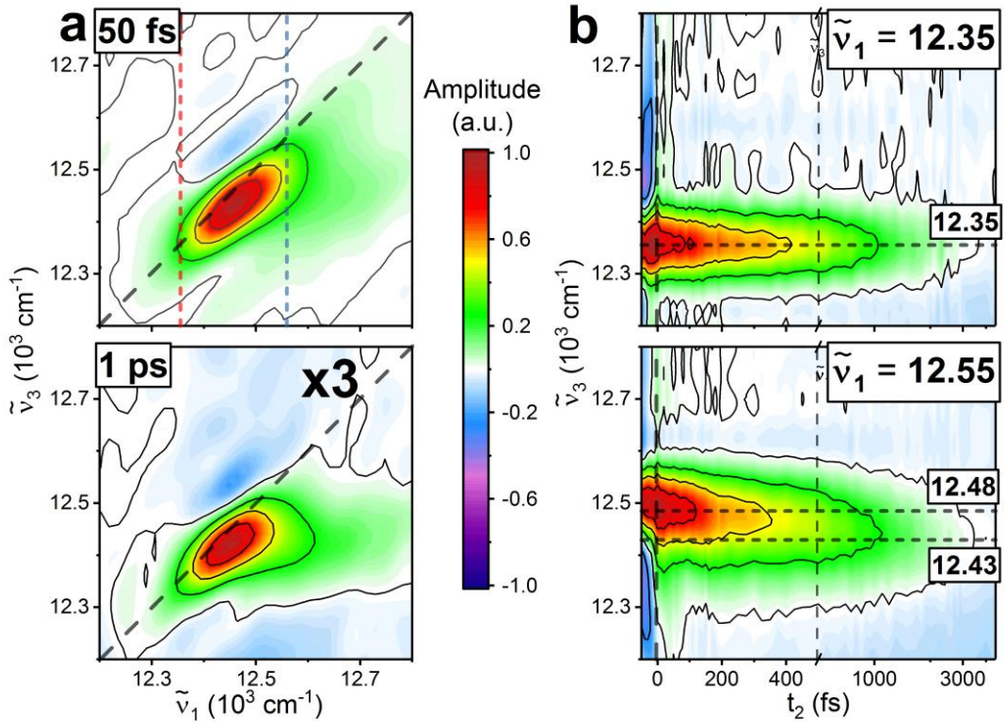

Figure 3: a) Absorptive MA 2DES spectra in the B800 spectral region at 50 fs (top) and 1 ps (bottom) population time. **b**) Extracted cuts from 2D spectra corresponding to TA spectra along the low-excitation-energy, red line in **a** (top), and the high-excitation-energy, blue line (bottom). Dashed horizontal lines in **b** indicate the initial and final wavenumber of the signal maximum.

The B800 ring system found in the LH2 complex of *Rh. acidophila* forms a C_9 symmetric "ring" of almost isolated BChl a pigments. The electronic coupling between these pigments (20-30 cm^{-1})[34] – is relatively weak compared to typical interaction energies with the bath, and the usual assumption is that the eigenstates are localized on individual pigments. This is in qualitative agreement with low-temperature single-molecule (SMS)[35] and spectral hole-burning (HB)[36] studies, which indicate that optical transitions to B800 are to a series of distinct states with properties analogous to that of BChl a, albeit shifted to slightly lower energy[37]. In these experiments, the (homogeneous) spectral linewidths - at least at the spectral red edge – appear largely limited by the B800->B850 transfer.

In terms of dynamics, a direct consequence of these narrow lines at low temperatures is that spectral overlap integrals become very small and intraband transfer in B800 cannot easily be reconciled with purely Förster-type incoherent energy transfer[38]. This could be expected qualitatively, as the modest intraband electronic coupling is still approximately 20% of the estimated low-temperature site-energy distribution of only 130 cm^{-1},[38] and not negligibly small.

Although studied also with time-resolved methods, B800 has been under less intense scrutiny than the more strongly coupled B850 ring – with much of the work being in the context of B800→B850 energy transfer rather than intraband dynamics. While several studies have targeted the intraband dynamics[39-44], the inherent difficulty in generating laser pulses short enough to resolve the dynamics

without increasing the spectral bandwidth enough to lose the necessary spectral resolution is likely at least partly behind the smaller total body of work. Here, we are primarily interested in exactly these intraband dynamics, the analysis of which 2DES is uniquely suited for[45].

In Figure 3a we show absorptive 2DES spectra of the B800 region at two selected population times. Visual inspection of these reveals good agreement with lineshapes found in earlier work[46]. The main feature is elliptical and strongly elongated along the diagonal shape, directly reflecting the significant inhomogeneous distribution in the system (see Figure S2). The photoinduced dynamics in the ring are directly observable through two characteristics: *i)* an overall loss of signal amplitude on a timescale of ~1 ps, and *ii)* spectral diffusion, i.e. an increasingly round peak shape at longer population times, the evolution taking place on a timescale of several hundred fs. We can straightforwardly assign these two transient features to B800→B850 transfer and B800 intraband relaxation, respectively.

Closer inspection of the spectra reveals that this "spectral diffusion" is far from uniform over the diagonal peak, as would be expected for a single transition. The peak shape at 1 ps in Fig. 3a is distinctly different from typical bath-fluctuation induced loss of correlation between excitation- and detection- frequencies in 2-level systems[47]. Instead, excitation- and detection- frequencies remain essentially completely correlated over the B800 lifetime at the red side of the band. At the blue side however, the stimulated emission signal amplitude moves from the diagonal towards the spectral center-of-mass. The latter demonstrates downhill energy-transfer within the B800-ring. The simultaneous loss of signal at the diagonal during this transfer reveals that the "donor" and "acceptor" states do not have significant spatial overlap and therefore are not correlated, as predicted by the weak pigment-pigment coupling. This corresponds qualitatively (but, as noted above, not *quantitatively*) to a Förster-transfer picture for energy transfer within the B800 ring.

Quantitative information about such excitation-frequency dependent dynamics is most efficiently extracted by "slicing" of the 2D spectra into a set of TA-like spectra at different $\tilde{\nu}_1$ (excitation) frequencies. In accordance with earlier terminology, we will refer to these spectra as "transient hole-burning spectra"[48] (THBS). This generates a dataset similar to pump-frequency dependent TA experiments, but circumvents the laser pulses related Fourier limit to the frequency/temporal resolution. We hasten to note that the experiment does not directly correspond to spectral hole-burning, as it is performed using broadband pulses and well within the perturbative regime. With the $\tilde{\nu}_1$ resolution of the 2DES experiment, we here create a stack of THBS's across the B800 band with 35 cm^{-1} spacing.

In Figure 3b we show time evolution of two representative examples – taken at the red and blue spectral edge, respectively, as indicated in Figure 3a. At the red edge, the spectral center of mass does not move and the lineshape remains almost static and narrow – here signal decay is due to the B800→B850 transfer. At the blue edge, in contrast, the lineshape is relatively broad and the spectrum shifts noticeably towards lower energies over the B800 lifetime. This relaxation is not to the bottom of the B800 band, however, but rather to the center-of-mass. The implication being that intraband relaxation is incomplete, and thus that relaxation within the B800 band is eventually outcompeted by the B800→B850 transfer.

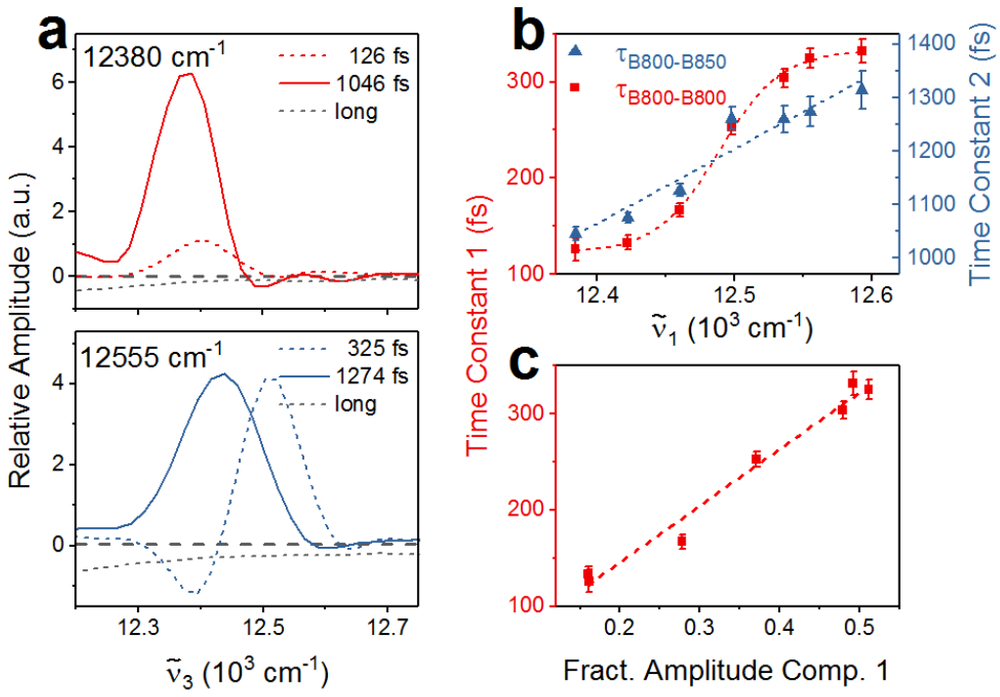

Figure 4: Global analysis of the B800 dynamics **a)** Decay associated spectra (DAS) of the 2D slices extracted at the red (top) and blue (bottom) edge of the B800 band. All global fits need three components, of which one is a broad negative-amplitude feature extending towards lower energies associated with the long-time decay of the B850 ESA (shown as dashed grey lines in figures **a**). We observe a general increase in time constants in conjunction with increasing relative amplitude of the shorter lifetime component at higher excitation frequencies. **b)** The time-constants of the intra- (1) and inter-band (2) components as a function of excitation ($\tilde{\nu}_1$) frequency. Sigmoidal (red) and linear (blue) fits to the data are shown to guide the eye. **c)** Time-constant (1) of the fast intra-band component as a function of its fractional amplitude-contribution to the global fit. Error bars displays the time-constant standard error as extracted from the global kinetic fit.

Quantitative analysis of these relaxation dynamics is possible through kinetic fitting of the THBS dynamics. Using a standard global analysis approach[49], we analyze all THBS individually using a sum-of-exponential decays model, and extract the decay-associated spectra (DAS) of each component. For each THBS with excitation wavenumber in the range of 12380 – 12600 cm^{-1} three unique components are necessary to describe the dynamics, two of which are related to B800 dynamics, while the third effectively describes the dynamics of the blue edge of the B850 excited state absorption (ESA) as will be discussed below. We note that this is an *effective* model of the relaxation dynamics, and the individual components do not necessarily correspond directly to particular physical processes.

Figure 4a shows the lifetimes and related DAS for the THBS depicted in Figure 3b. The differences in dynamics as a function of excitation frequency are clear: at red-edge excitation (higher panel in Figure 4a) we observe only a small loss of signal intensity at higher energy, with no distinguishable features suggesting downhill energy-transfer, which would appear as negative amplitude at the lower-energy side. After blue-edge excitation however, (lower panel in Figure 4a) downhill energy transfer contributes significantly as witnessed by the appearance of corresponding negative amplitude and shift of the central frequency in DAS.

The time-constants extracted from the global fits at excitation frequencies shown in Figure 4b follow a trend agreeing with this observation. The longer decay component, assigned to B800-B850

transfer, displays a linear time-constant increase across the band – the more red-detuned the excitation, the faster the transfer to B850. In contrast, the faster component shows an approximately bimodal behavior with time constants of about 120 fs at the red-edge and 330 fs at the blue edge. As shown in Figure 4c, this time-constant increase is concomitant with an increase in relative amplitude of this component. The most straightforward interpretation of this behavior is to assign the low-amplitude 120 fs decay at the red-edge to electronic relaxation in the immediate environment of the BChl a pigments (inertial solvation). While this weak component is likely present also at higher excitation frequencies, it becomes difficult to resolve when the 330 fs component increases in amplitude.

This longer component is clearly partly related to intraband relaxation; however, the DAS spectral shape – with much larger positive than negative amplitude – implies a simultaneous overall loss of B800 population. This is not surprising, in that it only means that a given B800 state has a probability to relax both to other B800 states (potentially with different transition dipole strength) and to states in the B850 band, as one would expect.

Comparison with the only weakly excitation-frequency dependent grow-in dynamics at the B800-B850 cross-peak (Figure S3), in conjunction with the observation that the average B800 lifetime does not increase at higher excitation frequencies (Figure S4), reveals that this "cross-talk" between decay components is fairly significant. This is in accord with early experimental[50] and theoretical[51] work, pointing to an interplay between B800 intraband and B800-B850 interband dynamics. Regardless, we can conclude from these data that transfer within the B800 ring occurs predominantly after excitation at the blue edge of the band, and that the time-constant for this transfer process is in the order of several hundred femtoseconds.

More direct information on intraband relaxation is available from polarized experiments. As the polarization of the signal – e. g. the pump-probe anisotropy – is independent of the total signal amplitude, it should in general be possible to isolate the intraband dynamics from interband relaxation. We show representative anisotropy decays extracted from polarized THBS of the B800 band in Figure 5a. We note immediately that the time zero anisotropy appears to be unusually large (i.e. >0.4). This is also the case in the polarized transient absorption spectrum of this LH2 species (see Figure S4). While it is possible to find anisotropies substantially higher than the typical maximal expected value of 0.4 after excitation of coherent superpositions of eigenstates[52, 53], we find it unlikely that this is could be a substantial contribution after ~100 fs. In particular, this would require such coherent superpositions to be maintained for the entire B800 lifetime, which is clearly not tenable. A more likely explanation is spectral overlap between ground state bleach (GSB) and stimulated emission (SE) transitions with ESA transitions with dipole orientations not parallel to GSB and SE. As shown in Figure S6, a relatively minor contribution from *e.g.* B800 biexiton ESA transitions is sufficient to cause the increased anisotropy observed here. However, as we are interested in the rate of depolarization rather than its absolute value, the details of this interpretation has little influence on the extracted physical picture.

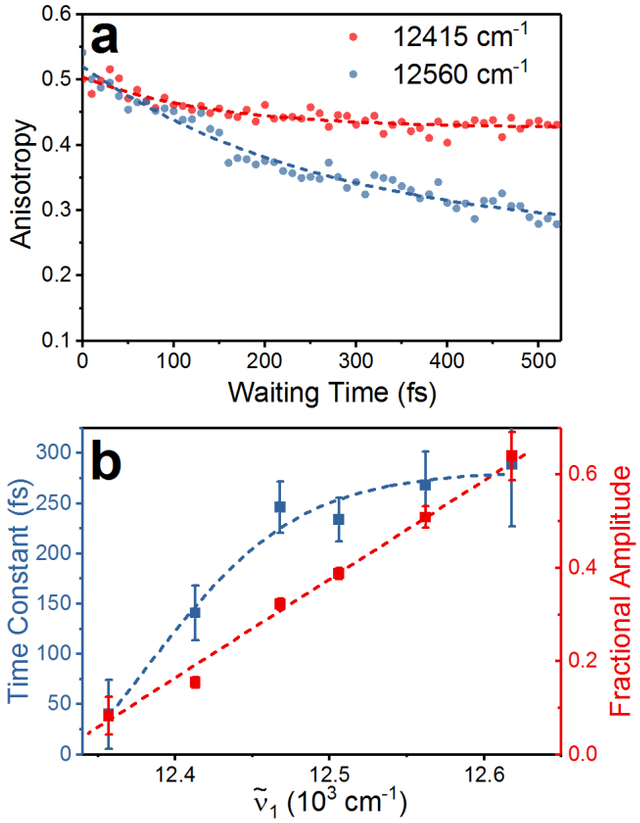

Figure 5: a) Time-dependence of the pump-probe anisotropy at representative red- (12415 cm^{-1}) and blue (12560 cm^{-1}) B800 edge excitation frequencies. The anisotropy decays are bi-exponential at all excitation frequencies, with the longer component exceeding the B800->B850 transfer time. Both anisotropy traces extracted from the respective signal maxima. **b)** time constant (blue) and fraction of the total decay amplitude (red) of the short time component in the anisotropy decay at a series of excitation frequencies. Sigmoidal (blue) and linear (red) fits to the data are shown to guide the eye.

In observing the anisotropy decays as a function of excitation frequency, we again find significant differences in apparent relaxation rates – in qualitative agreement with the global kinetic analysis of the THBS presented in Figure 4. Two representative decays are shown in Figure 5a, where one finds substantially faster depolarization at the blue edge of the B800 band. At all excitation frequencies, the decays are bi-exponential - with the longer-lived component extending well beyond the B800 lifetime. After red-edge excitation, the amplitude of this long-lived component dominates, and the anisotropy is essentially stationary. This implies that these relatively low-energy excitons are immobile, while the faster decay at the blue edge implies that high-energy excitons are mobile at least within some limited range. This effect is expected in an energetically disordered aggregate: at low energy nearest neighbor hopping is inhibited, as the "neighbor states" are likely to be higher in energy. Conversely, higher energy excitons are likely to have lower energy neighbors, and exciton transfer becomes favorable. The time-constant of the anisotropy decay of ~300 fs at high energies agrees qualitatively with the ~330 fs relaxation times extracted from global kinetic analysis of the THBS, in sum yielding a consistent intraband transfer rate of approximately 300 fs. This timescale is comparable to earlier TA work that investigated the B800 intraband dynamics[39, 41], where also the general transfer rate decrease at the spectral red edge was observed, but somewhat faster than

what was observed in recent work where the excitation frequency dependence was not considered in detail[43, 44]

Dynamics in the Strongly Coupled B850 Ring

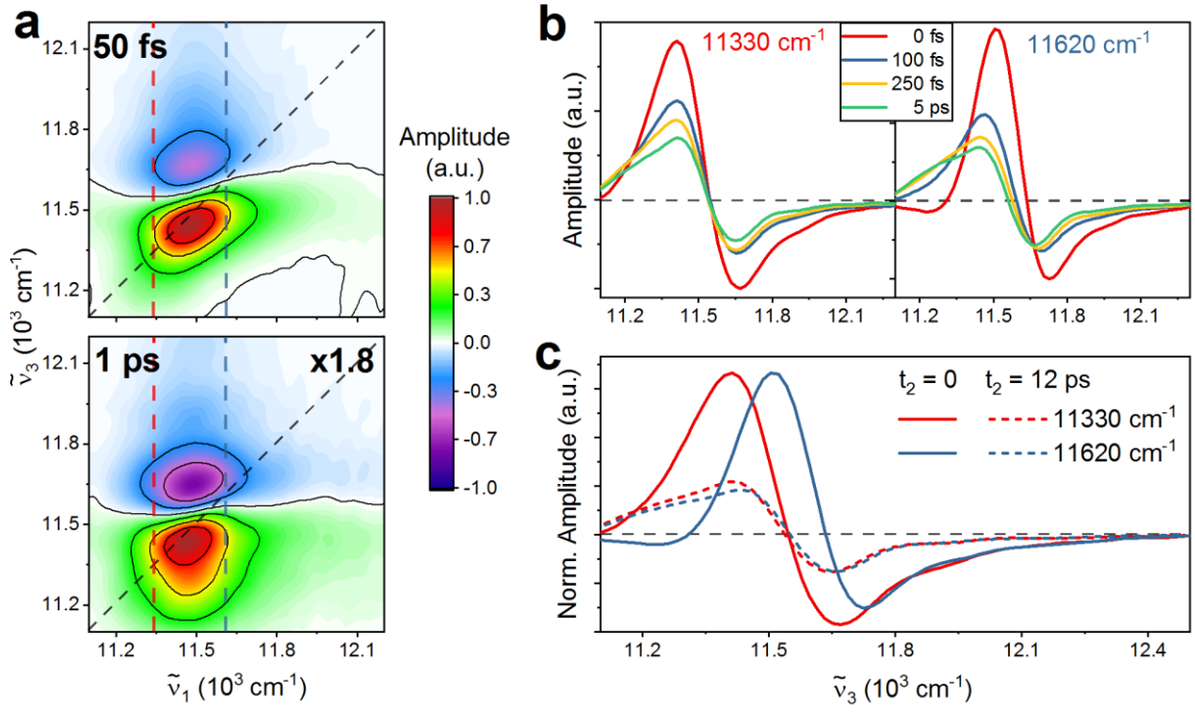

Figure 6: a) Absorptive MA 2DES in the B850 region at 50 fs (top) and 1 ps (bottom) population time. **b)** THBS extracted from the red (left) and blue (right) edge of the B850 band. At both excitation frequencies we observe almost complete relaxation to a broad-spectrum at the red side within a few hundred fs. **c)** Comparison of THBS extracted along the red- and blue- vertical lines in **a** at early (solid line) and late (dashed line) times. Spectra were normalized to the maximum amplitude of the early-time spectra. Note the coincidence of the blue side of the spectra at early times, and very similar spectra at long times.

As a consequence of the much higher density of states and the stronger electronic coupling, the dynamics in the B850 ring deviates strongly from that of B800. The inter-pigment coupling is one order of magnitude stronger than for the B800 ring (~200-400 cm^{-1} for the αβ pair in B850)[34]. This leads to much faster dynamics, and thus an increase in the homogeneous linewidth due to increased lifetime broadening (see supplementary Figures S8-S12). Even in low-temperature single-molecule experiments, the individual states appear effectively indistinguishable and the linear spectra are characterized by two to three broad lines[54] – in qualitative agreement with a Bloch-wave picture where all oscillator strength is concentrated in $k^{+/-1}$ collective states.

We show representative early- and late- time absorptive MA 2DES spectra in Figure 6a. The spectral shapes are qualitatively similar to time-resolved spectra of a wide range of natural[55, 56] and artificial[57, 58] structures of "J-aggregate" type. Along the diagonal, we observe the strong positive GSB/SE feature related to the optically bright excitons in the system. This feature is strongly overlapped at the high-energy side by a negative above diagonal ESA, related to transitions to two-exciton states. The small shift between excitonic and two-excitonic transitions complicates lineshape analysis, as the spectra become strongly congested, in particular in the regions near the resulting nodal line. The two-exciton transitions do not appear to be strongly correlated with the exciton transition frequency, as seen by the modest diagonal tilt of the ESA even at early times. This

results in cancellation of on-diagonal signals at higher frequencies, as is also observed for cyanine-dye based J-aggregates[59]. This implies that the two-exciton transition frequencies are only slightly sensitive to exactly which excitonic state in the manifold is populated.

The elongation of the main B850 diagonal feature at early times is a sign of significant heterogeneity in the system. Intraband relaxation following excitation rapidly washes out the correlation between excitation- and detection- frequencies within a few hundred fs. The correlation loss can be quantified *e.g.* by considering the slope of the nodal line between GSB/SE and ESA features, which here decreases initially with a 60 fs time-constant, followed by much slower long-time dynamics (see supplementary Figure S13). This spectral diffusion is accompanied by a noticeable overall red-shift of the band, resulting in the appearance of the positive signal amplitude in the 11 250 cm^{-1} region.

The intraband relaxation dynamics are intricate. To arrive at a consistent picture, we again perform detailed analysis of THBS at a range of $\tilde{\nu}_1$ frequencies covering the entire B850 band. Figure 6b shows THBS extracted from the red and blue edges of the absorption band. As a common feature for all THBS regardless of excitation frequency, and in agreement with the TA data (Figure 1b), the spectrum at early times is dominated by a relatively narrow and intense GSB/SE feature overlapping a broad ESA signal on the higher frequency side. The intensity of this signal decreases rapidly, followed by a red-shift and broadening of the positive signal components. The rapid intraband relaxation is obvious, as it is clear that – regardless of initial excitation frequency – the system reaches a relaxed quasi-equilibrium state within a few hundred fs. Comparing the normalized late-time THBS for different $\tilde{\nu}_1$ frequencies in Figure 6c, it is additionally clear that this relaxed state is independent of excitation frequency: all initial conditions result in rapid population of the same lowest-energy state(s). This stands in contrast to the B800 dynamics, where intraband relaxation never reaches completion due to the comparable timescales of intra- and inter- band transfer.

While assigning the appearance of a red-shifted spectrum at late times to an excited-state relaxation process is appealing, red-edge excitation (Figure S7 and red line in Figure 6c) allows direct population of the relevant state from the ground-state. As such, the "shoulder" around 11 250 cm^{-1} in Figure 6c does not appear to be purely SE signal originating from a dynamic Stokes shift process, but is rather a signal associated with the lowest energy state in the B850 manifold. These states have been observed earlier in spectral hole-burning experiments[22], where a distribution of weak transitions were observed in the red tail of the absorption band.

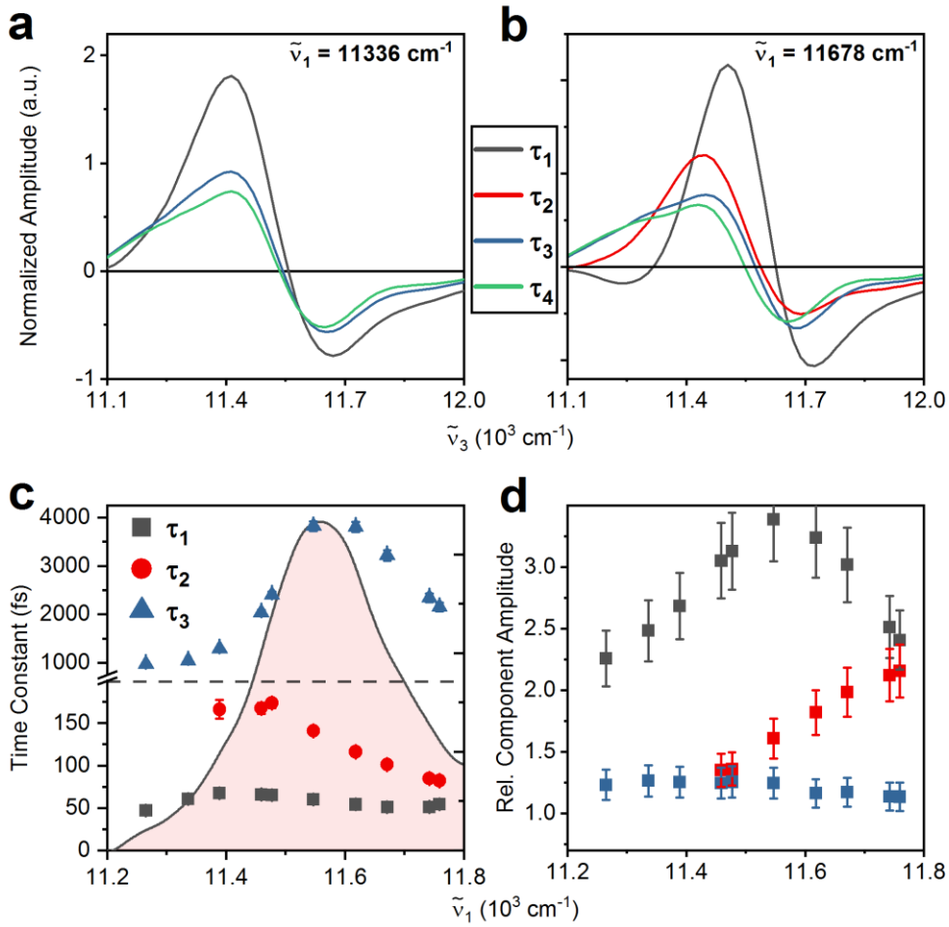

Figure 7: Global kinetic fits to the B850 intraband relaxation dynamics. **a)** Evolution associated spectra (EAS) extracted from the spectral red edge (11 336 cm^{-1}). **b)** EAS extracted from the spectral blue edge (11 678 cm^{-1}). Note that at excitation frequencies of ~11400 cm^{-1} and above four components are needed for a satisfactory fit, while three components are sufficient at lower frequencies. **c)** Component lifetimes extracted from THBS dynamics as a function of excitation frequency ($\tilde{\nu}_1$). Overlaid with the absorption spectrum in the B850 region (shaded red area). The long-lived component corresponding to the ground-state recovery (τ_4 in **a** and **b**) is omitted for clarity. **d)** Ratios of decay component amplitudes relative to the amplitude of long-lived component associated with ground-state recovery (τ_4). Error bars estimated to +/-10% of the reported values.

The quantitative relaxation dynamics within the B850 band can be addressed using a global kinetic analysis scheme similar to that used for the B800 dynamics above. The dense manifold of exciton states within which the relaxation takes place is not very amenable for analysis using kinetic level-to-level transfer models, however. Since the individual excitonic states are not spectrally resolvable, a sum-of-exponential global fit to the dynamics will only result in a model of "effective dynamics" between "effective states". Nevertheless, global kinetic analysis provides valuable information about relaxation timescales.

As illustrated in Figure 7a and b, the excitation relaxation network is somewhat excitation frequency dependent: at lower energies, we find that three components are required to fit the dynamics, whereas at higher energies we need four components in total. The final decay component is always the ground-state recovery time of the system (corresponding to timescale of hundreds of

picoseconds). As we concentrate on the intraband relaxation represented by the faster decay components, we do not address this in the following.

The relaxation dynamics involve continuous spectral shifts in addition to changes in amplitude, which makes the DAS representation of the component amplitudes used above inconvenient. Instead, we represent the decay amplitudes in terms of the *Evolution Associated Spectra* (EAS)[49]. In this model the decay is fit to a strictly sequential kinetic target model, where the population initially created in "state 1" transfers to "state 2", and so on. The EAS can be interpreted as the spectra of the "states" (or "compartments") in this sequential kinetic model, although it should be noted that these states do not generally represent actual eigenstates of the system. However, the time-constants involved are independent of the chosen representation of the spectral amplitudes.

In Figure 7a and b we show representative examples of EAS from red- and blue- edge excitation, respectively. The initial decay dynamics are clearly visible from the narrow, intense component 1 feature (black spectra), and the excitation-frequency dependent differences in the subsequent signal evolution also become clear. After red-edge excitation, the initially prepared state decays on a timescale of 50 fs to form the spectrum of an almost relaxed population (Figure 7a). After excitation at above ~11400 cm^{-1}, however, we observe the formation of an intermediate "species". This is characterized by a spectrum red-shifted relative to the initial state, but still spectrally narrow with no clear significant contribution of the characteristic low-frequency "shoulder" of the fully relaxed state (Figure 7b, red line). Only after this component has decayed, with a time constant in the range of 100 fs, does the relaxed-state-like spectrum appear. This suggests that relaxation channels exist after higher-frequency excitation that are not accessible after excitation at the red spectral edge. A likely interpretation is that this intermediate component is related to amplitude loss due to exciton motion on the ring.

The global analysis reveals that the time-constant associated with the initial decay is almost independent of excitation frequency, being approximately 50 fs across the absorption spectrum, as displayed in Figure 7c. Similar signal loss has been observed in TA[60] and transient grating experiments[24], as well as in respective simulations,[26] and has been interpreted as a characteristic of dynamic localization of the initial electronic wavepacket into the much smaller exciton. We can estimate the magnitude of this signal loss by comparing the EAS amplitude of the first component τ_1 with that of the component associated with ground-state recovery (τ_4). Hence, we compare the signal intensity of the initially prepared state with signal intensity of the fully relaxed excited state. In Figure 7d we show the ratio between the amplitude maxima of these components as a function of excitation frequency. This ratio – a measure for the extent of signal loss – clearly becomes larger towards the absorption maximum, where the density of states is highest. At these excitation frequencies, excitation involves a coherent superposition of the largest possible number of states (and thus the largest initial transition dipole moment), and as a consequence the largest loss of signal strength during localization of the exciton - assuming that the final state is independent of the initial excitation condition.

The association of the ~100 fs component with exciton motion is supported by the increase in amplitude and shortening of the time constant of this component at higher excitation frequencies – *i.e.* the implication that site-to-site motion becomes more important and faster as the initial state increase in energy. Note that this interpretation also suggests that site-to-site transfer may not be

efficient after red-edge excitation, leading to low exciton mobility and consequently less efficient energy transport at low temperatures.

We reiterate that after the decay of this intermediate component, a state is formed that appears spectrally very similar to the fully relaxed excited state. The EAS of this component is shown in blue in Figure 7a and b. The modest spectral changes (compare blue and green spectra in Figure 7a, b) and picosecond dynamics associated with this component suggest a connection with nuclear motion - *e.g.* relatively minor structural relaxation.

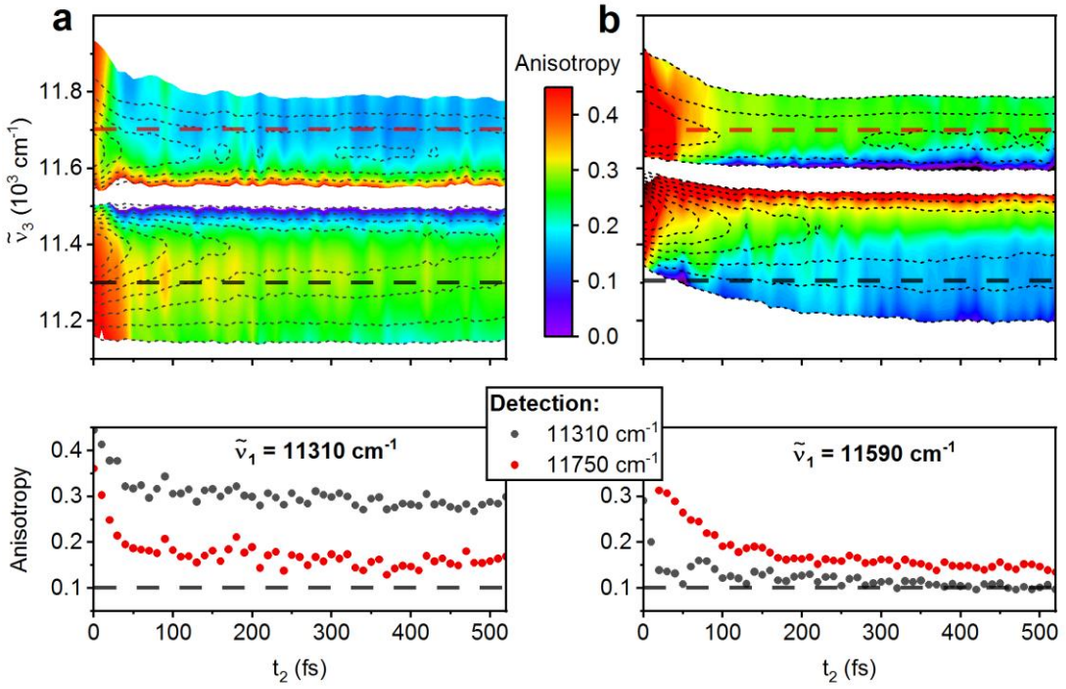

Figure 8: THBS anisotropy at **a)** red-edge (left) and **b)** blue-edge excitation. Color scale indicates anisotropy values and contour lines – isotropic signal amplitude. Single-point anisotropy traces extracted along the dashed horizontal lines are shown in the bottom panels. In the detection frequency ($\tilde{\nu}_3$) dispersed plots in the upper panels only areas with signal amplitude larger than 10% of the maximum amplitude of the magic-angle spectrum are shown.

As for the B800 ring above, we expect motion of the exciton in B850 to be associated with a loss of polarization. As an observable, this polarization loss is more closely associated with physical motion than the energy relaxation discussed above. In Figure 8 respectively, we show representative THBS anisotropy decays after red-edge and blue-edge excitation. Only data in regions where the isotropic signal strength is significant (>10% of maximum amplitude) are shown, as anisotropies for weak signals become highly unreliable. As such, *e.g.* the line of zero intensity between GSB/SE and blue-shifted ESA around 11 500 cm^{-1} is here masked. The starting anisotropy is initially decaying very rapidly regardless of excitation frequency, with slower subsequent dynamics. The fast depolarization timescale (~20-30 fs) is qualitatively comparable with the observed early-time signal intensity loss (~50 fs), which suggest at least partly a connection of this depolarization to dephasing of the initial electronic wavepacket.[60] Indeed, the time scale agrees with simulations of the coherent

contribution to the anisotropy decay[61].We note, however, that the depolarization timescale is close to the excitation-pulse cross-correlation, which makes reliable analysis difficult.

The time-evolution of the anisotropy following the initial fast dephasing contains valuable information about the relaxation mechanism in the system. In general, B850 is a two-dimensional system, *i.e.* the anisotropy should decay towards 0.1 as the exciton transition-moment direction randomizes during transfer around the ring. Transfer in an energy-landscape with significant static disorder is generally connected to energy-relaxation, and a direct correlation between the energy-relaxation dynamics and polarization loss is expected if "random walk" behavior is the dominant relaxation mechanism. At excitation frequencies at the absorption maximum and above, this observation largely appears to hold: as the detected isotropic signal (contour lines in Figure 8b) redshifts, the anisotropy decreases rapidly towards 0.1. Thus, when the excited state population arrives in the relaxed state (whose main spectral characteristics are in the 11 250 cm^{-1} region) it is already essentially entirely depolarized – *i.e.* the exciton has traveled some significant distance prior to arrival.

At excitation at approximately 11400 cm^{-1} and below, however, the picture is entirely different. Here, there is little – if any – depolarization subsequent to the initial ultrafast dephasing. In general, we find that depolarization is severely inhibited up to excitation frequencies of at least 11500 cm^{-1}, with the time required for depolarization decreasing monotonically with increasing excitation frequency (see supplementary Figure S14). The conclusion we draw is that relaxation after red-edge excitation at 11400 cm^{-1} and below involves on average (much) less than one energy-transfer step. Global kinetic analysis of population dynamics however, along with simple visual inspection of the unprocessed data, reveal that relaxation is nevertheless ultrafast and involves significant spectral changes. The lack of depolarization leads us to conclude that this relaxation is *local* and does not involve *e.g.* diffusion to a global minimum on a static disordered energy surface.

While not directly observable in our measurements, the fact that the excited-state population rapidly arrives to the same relaxed state regardless of excitation frequency suggests that dynamics also at higher excitation frequencies involve analogous local relaxation after an initial mobile phase. Therefore, one can speculate about the initial phase of energy relaxation being connected with exciton motion on the LH2 ring, where after the loss of sufficient energy the exciton becomes immobile and relaxes locally.

CONCLUSIONS

We have investigated the intraband relaxation in the B800 and B850 bands of LH2 from *Rh. acidophila* at 77 K temperature. The differences in exciton dynamics of two bands are substantial, as expected from the very different electronic coupling between pigments in the rings. The weak electronic coupling in the B800 band leads to relatively slow intraband exciton motion, which appears to be a factor 3 or 4 faster than the B800→B850 energy transfer timescale. Interestingly, the intraband relaxation does not reach completion due to the limited number of energy transfer steps possible within the B800 lifetime. At the same time, we find that static disorder in the band is likely substantially larger than the thermal energy at 77 K (~50 cm^{-1}), as intraband energy transfer appears to be essentially completely inhibited for states at the red edge of the absorption band.

The dynamics in the B850 band are more surprising. In accordance with earlier studies, we find that energy relaxation is very fast – mostly finished within a few hundred femtoseconds. Nevertheless, the lack of prominent depolarization reveals that states located at the red edge of the spectrum have very limited mobility. As is the case for B800, the lack of mobility can be understood as a consequence of large static disorder compared to the thermal energy. It is clear, however, that energy relaxation takes place not only through exciton diffusion in a disordered energy-landscape towards a global minimum. Instead, we find that a significant part of the relaxation is *local,* in that it involves no spatial motion of the exciton. What is still lacking is a clear understanding of this site-local energy relaxation mechanism, which appears to dissipate up to several hundred cm^{-1} of energy to yield relaxed quasi-equilibrium excited state on a timescale comparable to electronic decoherence. We expect that further experimental and theoretical work addressing this exciton trapping behavior under controlled circumstances could lead to a deeper understanding of the electronic structure and relaxation dynamics not only in LH2 but also in a wide range of extended soft-matter systems.

METHODS AND MATERIALS

Spectroscopy:

The instrument used for 2DES and degenerate TA experiments is described in detail elsewhere[62]. Here, we briefly summarize the key points: A 1030 nm Yb:KGW laser (Pharos, Light Conversion ltd.) was used to pump a lab-built noncollinear optical amplifier, the pulses of which were compressed by a combination of chirped mirrors and a fused silica prism compressor. The output was approximately 13 fs, ∼130 nm full width at half-maximum pulses with a spectrum centered at 830 nm. In order to avoid artifacts related to exciton-exciton annihilation, the pulse energy was kept at 600 pJ for 2DES and 750 pJ for degenerate TA measurements. The beams were focused into a 160 μm diameter spot in the sample. All experiments were done at 20 kHz repetition rate. The coherence time was scanned from −230 to 500 fs in 2 fs steps, resulting in a spectral resolution of 33 cm^{-1} on the $\tilde{\nu}_1$ axis; the resolution on the $\tilde{\nu}_3$ axis was 58 cm^{-1}.

The linear polarizations of the pulses were independently controlled by a combination of a quarter-wave plate and linear wire-grid polarizers in each beam. In order to avoid depolarization artifacts, we measure population dynamics at magic angle conditions (<54.7, 54.7, 0 ,0>), while anisotropies were calculated as usual as a combination of the <0, 0, 0, 0> and <90, 90, 0, 0> sequences of linearly polarized pulses.

Sample preparation:

LH2 from *Rh*. acidophila was extracted, isolated, and purified according to earlier detailed procedures[63]. The purified sample was stored at -40 degrees C in buffer until immediately before use. Prior to the experiment, the LH2 stock solution was diluted in TRIS-HCl buffer containing LDAO, glucose, glucose oxidase, and catalase. The resulting buffer solution was mixed to a 1:2 ratio with glycerol to reach an absorbance of ~0.2 in a 200 μm optical path cell, where after the sample was immediately inserted in a liquid nitrogen flow cryostat (Oxford Instruments) and kept at 77 K throughout the measurement.

SUPPLEMENTARY MATERIAL

Additional spectra, kinetic traces, time-evolution of anti-diagonal lines, and nodal line analysis.

ACKNOWLEDGEMENTS

The work was supported by Laserlab-Europe grant: EU-H2020, 654148, the Swedish Research Council, and Deutsche Forschungsgemeinschaft. RC acknowledges funding by BBSRC grant number BB/N016734/1. MS acknowledges financial support by the German Academic Exchange Service (Personal Scholarship 57210526). We thank Tomas Mancal and Maxim Gelin for helpful discussions.

DATA AVAILABILITY

The data that support the findings of this study are available from the corresponding author upon reasonable request.

CONFLICTS OF INTEREST

The authors declare no conflicts of interest

REFERENCES

[1] R. E. Blankenship, *Molecular mechanisms of photosynthesis* (Wiley/Blackwell, Chichester, West Sussex, 2014), Second edition. edn.,
[2] K. Wohl, New Phytologist **39** (1940) 33.
[3] G. H. Schmid, and H. Gaffron, Plant Physiol **S 43** (1968) S29.
[4] T. Renger, V. May, and O. Kuhn, Phys Rep **343** (2001) 138.
[5] C. J. Law *et al.*, Mol Membr Biol **21** (2004) 183.
[6] H. van Amerongen, L. Valkunas, and R. van Grondelle, *Photosynthetic Excitons* (World Scientific: Singapore, 2000),
[7] V. Perlik *et al.*, J. Chem. Phys. **142** (2015)
[8] V. P. Singh *et al.*, J. Chem. Phys. **142** (2015)
[9] A. Ishizaki, and G. R. Fleming, J. Chem. Phys. **130** (2009)
[10] L. P. Chen *et al.*, J. Chem. Phys. **131** (2009)
[11] C. Curutchet, and B. Mennucci, Chem. Rev. **117** (2017) 294.
[12] R. G. Saer, and R. E. Blankenship, Biochem. J **474** (2017) 2107.
[13] G. Mcdermott *et al.*, Nature **374** (1995) 517.
[14] K. Timpmann, N. W. Woodbury, and A. Freiberg, J. Phys. Chem. B **104** (2000) 9769.
[15] S. Hess *et al.*, Proc. Natl. Acad. Sci. U.S.A. **92** (1995) 12333.
[16] J. T. M. Kennis *et al.*, J. Phys. Chem. B **101** (1997) 7827.
[17] H. M. Wu *et al.*, J. Phys. Chem. B **101** (1997) 7654.
[18] S. Georgakopoulou *et al.*, Biophys. J. **82** (2002) 2184.
[19] S. J. Jang, and R. J. Silbey, J. Chem. Phys. **118** (2003) 9324.
[20] A. M. van Oijen *et al.*, Science **285** (1999) 400.

[21] D. Leupold *et al.*, Phys. Rev. Lett. **77** (1996) 4675.
[22] A. Freiberg *et al.*, J. Phys. Chem. B **107** (2003) 11510.
[23] T. Polivka *et al.*, J. Phys. Chem. B **104** (2000) 1088.
[24] L. D. Book *et al.*, J. Phys. Chem. B **104** (2000) 8295.
[25] T. Pullerits, M. Chachisvilis, and V. Sundstrom, J. Phys. Chem. **100** (1996) 10787.
[26] O. Kuhn, and V. Sundstrom, J. Chem. Phys. **107** (1997) 4154.
[27] S. J. Jang, and B. Mennucci, Rev Mod Phys **90** (2018)
[28] G. Trinkunas *et al.*, Phys. Rev. Lett. **86** (2001) 4167.
[29] M. Dahlbom *et al.*, J. Phys. Chem. B **105** (2001) 5515.
[30] V. Nagarajan *et al.*, Proc. Natl. Acad. Sci. U.S.A. **93** (1996) 13774.
[31] R. Kunz *et al.*, Biophys. J. **106** (2014) 2008.
[32] M. Ratsep *et al.*, J. Chem. Phys. **141** (2014)
[33] R. Kunz *et al.*, J. Phys. Chem. B **116** (2012) 11017.
[34] S. Tretiak *et al.*, J. Phys. Chem. B **104** (2000) 9540.
[35] C. Hofmann *et al.*, New J Phys **6** (2004)
[36] D. Grozdanov *et al.*, J. Phys. Chem. B **114** (2010) 3426.
[37] M. Ratsep *et al.*, J. Chem. Phys. **134** (2011)
[38] A. M. van Oijen *et al.*, Biophys. J. **78** (2000) 1570.
[39] S. Hess *et al.*, Biophys. J. **69** (1995) 2211.
[40] J. M. Salverda *et al.*, J. Phys. Chem. B **104** (2000) 11395.
[41] M. Wendling *et al.*, Biophys. J. **84** (2003) 440.
[42] V. Novoderezhkin, M. Wendling, and R. van Grondelle, J. Phys. Chem. B **107** (2003) 11534.
[43] J. I. Ogren *et al.*, Chem Sci **9** (2018) 3095.
[44] A. L. Tong *et al.*, J. Phys. Chem. B **124** (2020) 1460.
[45] D. M. Jonas, Annu. Rev. Phys. Chem. **54** (2003) 425.
[46] M. Ferretti *et al.*, Sci Rep-Uk **6** (2016)
[47] M. H. Cho, Chem. Rev. **108** (2008) 1331.
[48] P. Hamm, and M. T. Zanni, *Concepts and methods of 2d infrared spectroscopy* (Cambridge University Pres, Cambridge ; New York, 2011),
[49] I. H. M. van Stokkum, D. S. Larsen, and R. van Grondelle, Bba-Bioenergetics **1657** (2004) 82.
[50] H. M. Wu *et al.*, J. Phys. Chem. **100** (1996) 12022.
[51] O. Kuehn, and V. Sundstroem, J. Phys. Chem. B **101** (1997) 3432.
[52] K. Wynne, and R. M. Hochstrasser, Chem. Phys. **171** (1993) 179.
[53] E. R. Smith, and D. M. Jonas, J. Phys. Chem. A **115** (2011) 4101.
[54] M. Ketelaars *et al.*, Biophys. J. **80** (2001) 1591.
[55] J. Dostal *et al.*, J Am Chem Soc **134** (2012) 11611.
[56] S. H. Sohail *et al.*, J. Chem. Phys. **147** (2017)

[57] J. Dostal *et al.*, Nat. Commun. **9** (2018)
[58] J. Lim *et al.*, Nat. Commun. **6** (2015)
[59] F. Milota *et al.*, J Phys Chem A **117** (2013) 6007.
[60] V. Nagarajan *et al.*, Proceedings of the National Academy of Sciences **93** (1996) 13774.
[61] O. Kuhn, V. Sundstrom, and T. Pullerits, Chem. Phys. **275** (2002) 15.
[62] R. Augulis, and D. Zigmantas, Opt. Express **19** (2011) 13126.
[63] A. T. Gardiner, D. M. Niedzwiedzki, and R. J. Cogdell, Faraday Discuss. **207** (2018) 471.

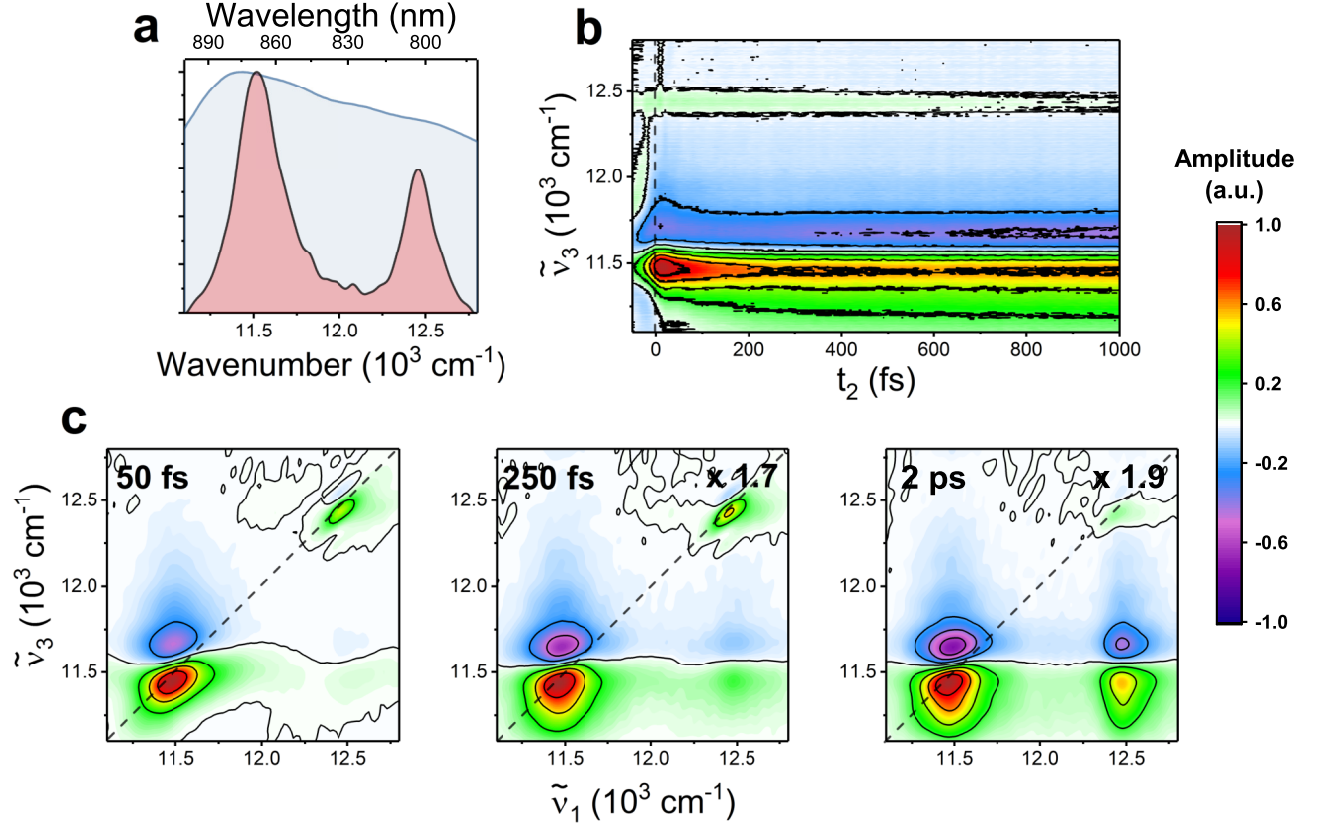
a
Wavelength (nm)
890
860
830
800
11.5
12.0
12.5
Wavenumber (10^3 cm^{-1})
b
12.5
12.0
11.5
$\tilde{\nu}_3$ (10^3 cm^{-1})
0
200
400
600
800
1000
t_2 (fs)
Amplitude (a.u.)
1.0
0.6
0.2
-0.2
-0.6
-1.0
c
50 fs
250 fs
x 1.7
2 ps
x 1.9
$\tilde{\nu}_3$ (10^3 cm^{-1})
$\tilde{\nu}_1$ (10^3 cm^{-1})

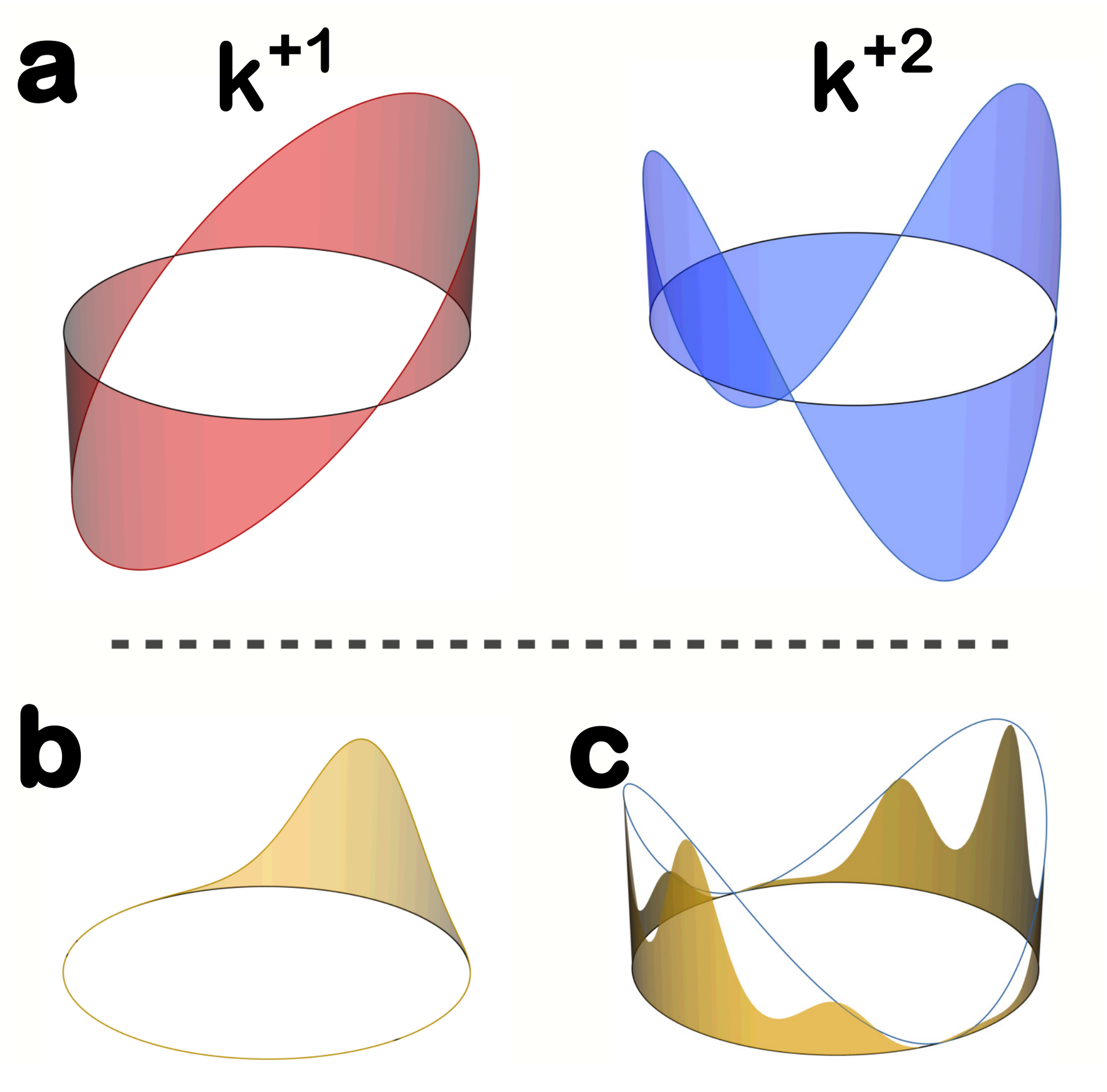
a
k+1
k+2
b
c

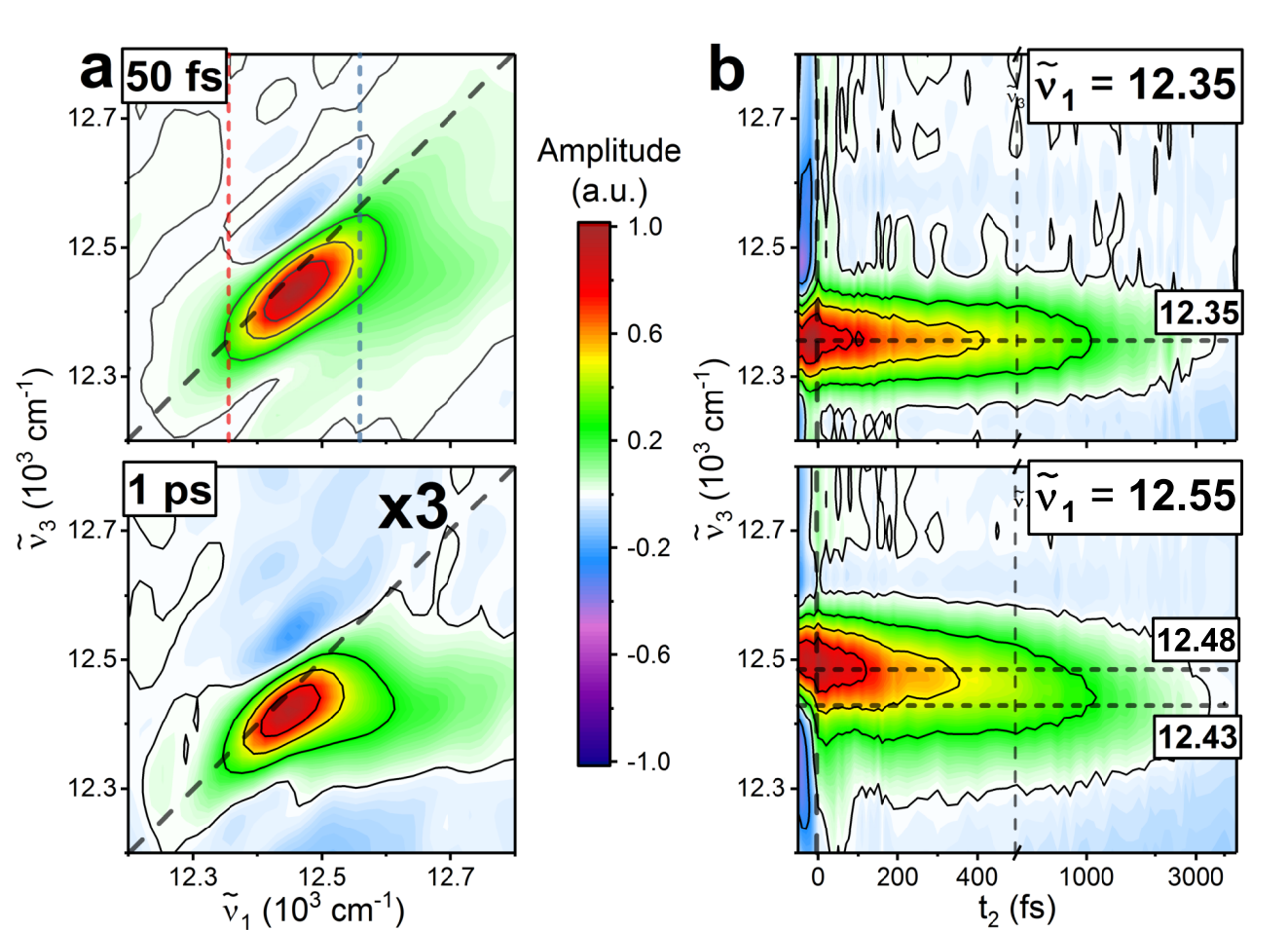
a
50 fs
1 ps
x3
b
$\tilde{\nu}_1$ = 12.35
$\tilde{\nu}_1$ = 12.55
12.35
12.48
12.43
Amplitude
(a.u.)
1.0
0.6
0.2
-0.2
-0.6
-1.0
$\tilde{\nu}_3$ (10^3 cm^{-1})
$\tilde{\nu}_1$ (10^3 cm^{-1})
t_2 (fs)
12.3
12.5
12.7
0
200
400
1000
3000

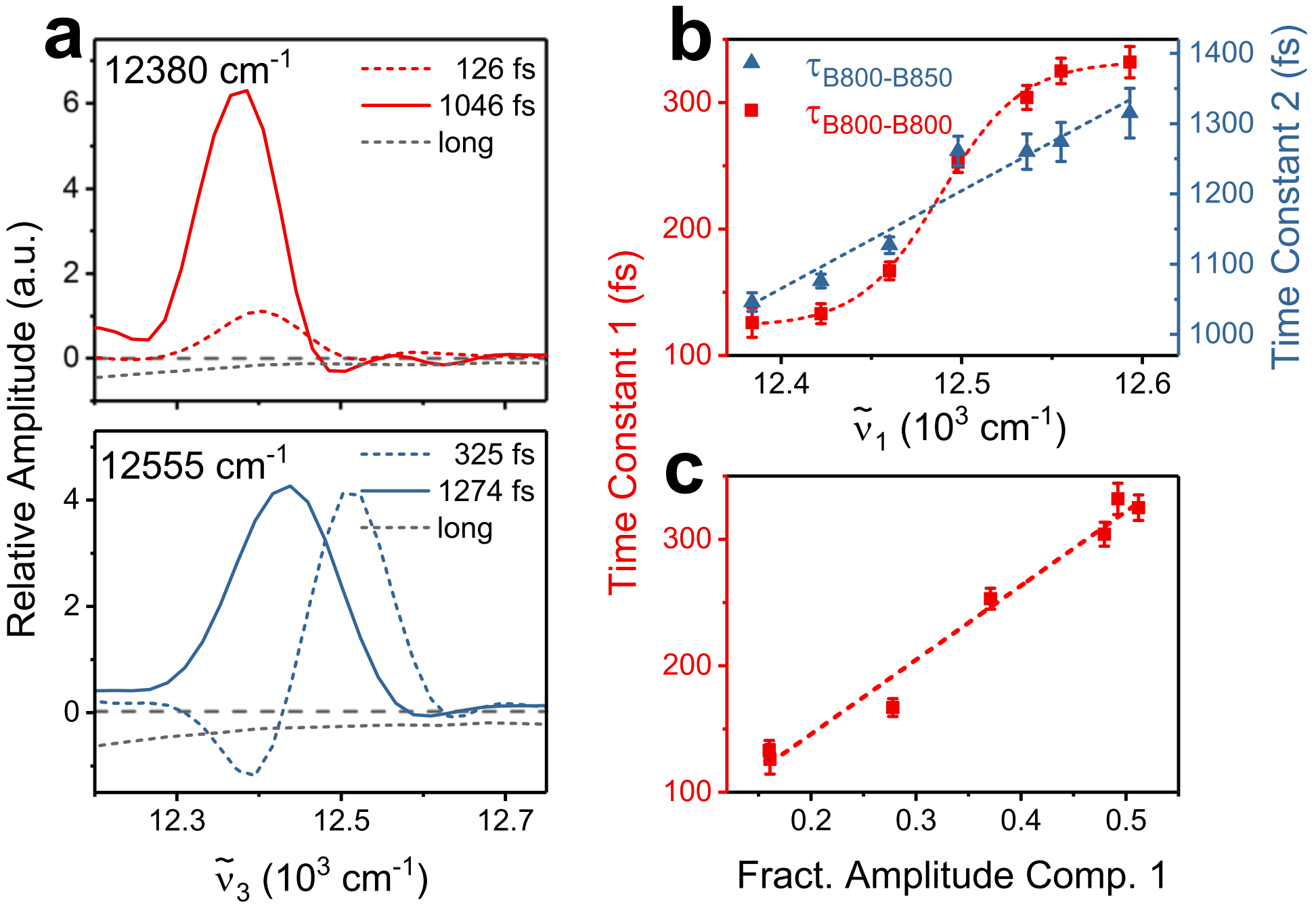
a
12380 cm-1
126 fs
1046 fs
long
12555 cm-1
325 fs
1274 fs
long
Relative Amplitude (a.u.)
ν̃3 (10^3 cm^-1)
b
τB800-B850
τB800-B800
Time Constant 1 (fs)
Time Constant 2 (fs)
ν̃1 (10^3 cm^-1)
c
Time Constant 1 (fs)
Fract. Amplitude Comp. 1

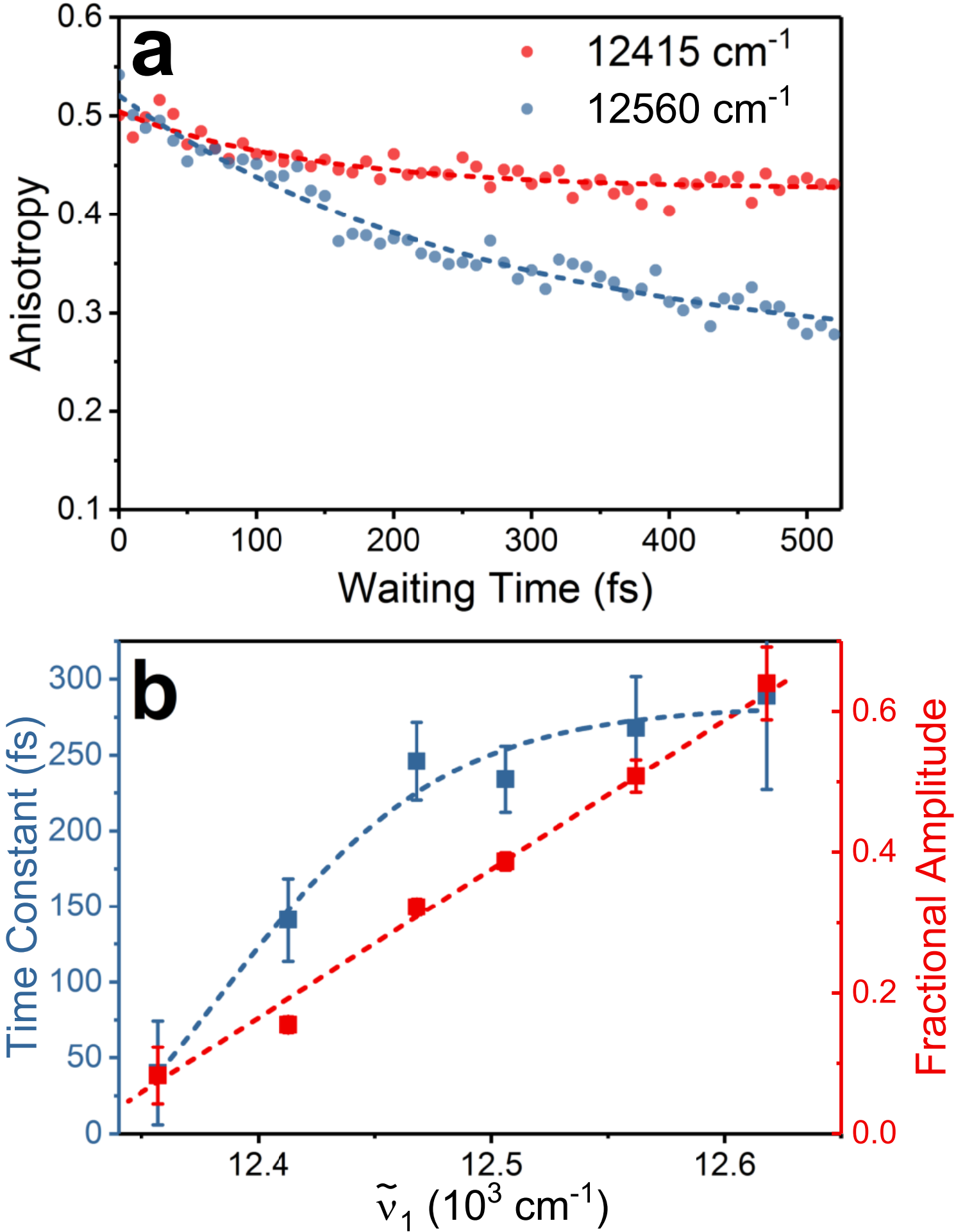
a
12415 cm-1
12560 cm-1
Anisotropy
0.6
0.5
0.4
0.3
0.2
0.1
0
100
200
300
400
500
Waiting Time (fs)
b
Time Constant (fs)
300
250
200
150
100
50
0
Fractional Amplitude
0.6
0.4
0.2
0.0
12.4
12.5
12.6
$\tilde{\nu}_1$ (10^3 cm^{-1})

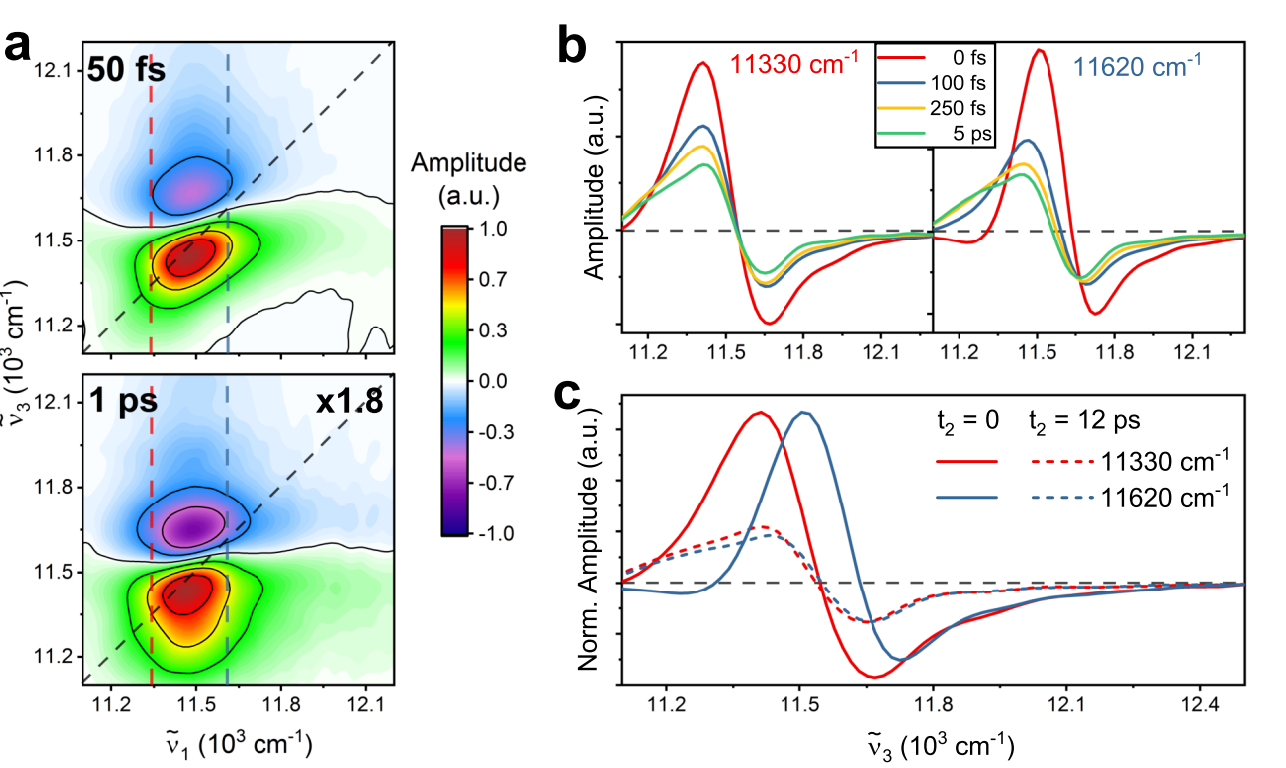
a
50 fs
1 ps
x1.8
12.1
11.8
11.5
11.2
$\tilde{\nu}_3$ (10^3 cm^{-1})
$\tilde{\nu}_1$ (10^3 cm^{-1})
Amplitude (a.u.)
1.0
0.7
0.3
0.0
-0.3
-0.7
-1.0
b
11330 cm^{-1}
11620 cm^{-1}
0 fs
100 fs
250 fs
5 ps
Amplitude (a.u.)
c
t_2 = 0
t_2 = 12 ps
11330 cm^{-1}
11620 cm^{-1}
Norm. Amplitude (a.u.)
12.4
$\tilde{\nu}_3$ (10^3 cm^{-1})

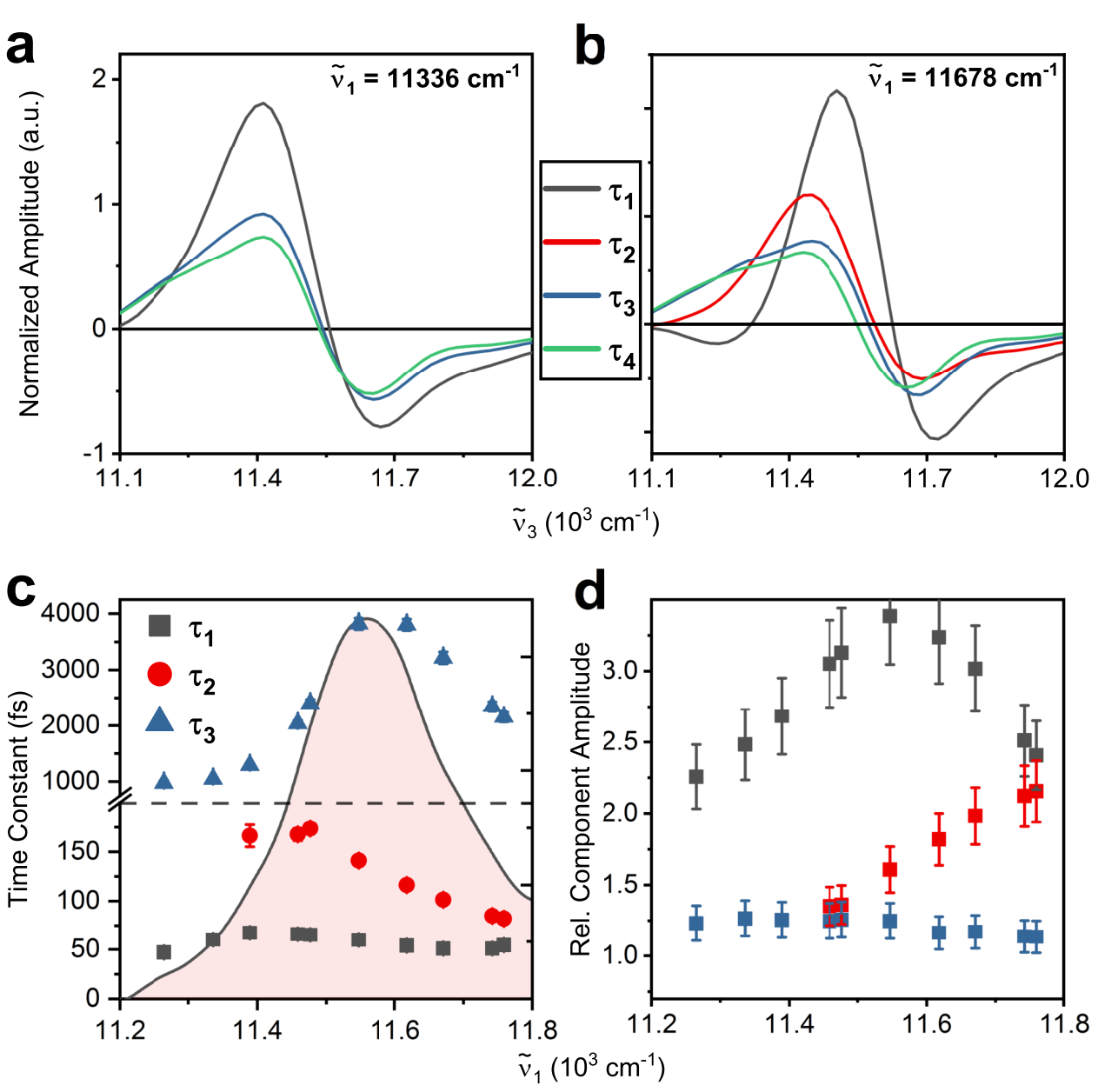
a
b
c
d
$\tilde{\nu}_1$ = 11336 cm^{-1}
$\tilde{\nu}_1$ = 11678 cm^{-1}
Normalized Amplitude (a.u.)
$\tilde{\nu}_3$ (10^3 cm^{-1})
τ_1
τ_2
τ_3
τ_4
Time Constant (fs)
Rel. Component Amplitude
$\tilde{\nu}_1$ (10^3 cm^{-1})

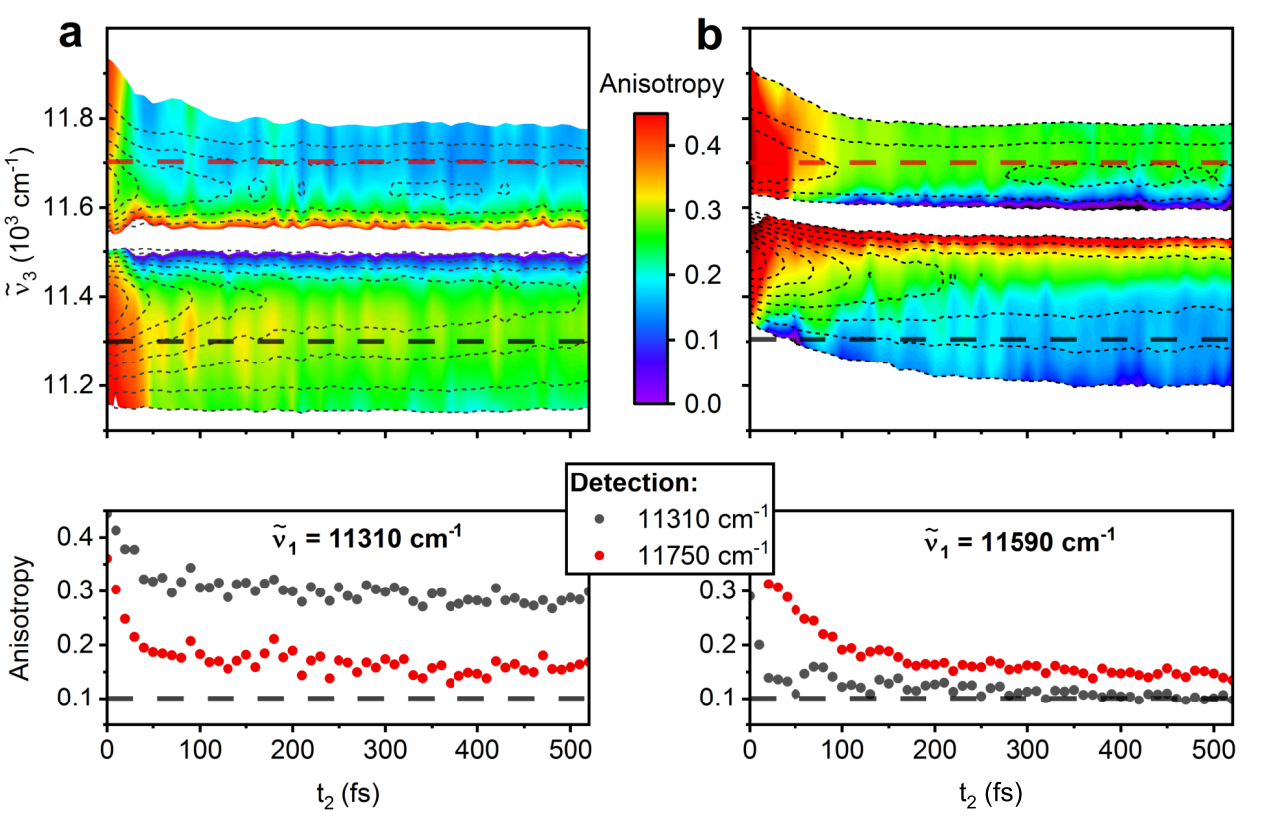
a
b
Anisotropy
0.4
0.3
0.2
0.1
0.0
$\tilde{\nu}_3$ (10^3 cm^{-1})
11.8
11.6
11.4
11.2
Detection:
11310 cm^{-1}
11750 cm^{-1}
$\tilde{\nu}_1$ = 11310 cm^{-1}
$\tilde{\nu}_1$ = 11590 cm^{-1}
Anisotropy
0.4
0.3
0.2
0.1
0
100
200
300
400
500
t_2 (fs)